

Supporting Information

Wearable high-dielectric-constant polymer with core-shell liquid metal inclusions for biomechanical energy harvesting and self-powered user interface

Shengjie Gao^{1,2}, Ruoxing Wang^{1,2}, Chenxiang Ma^{1,2,3}, Zihao Chen⁴, Yixiu Wang^{1,2}, Min Wu^{1,2}, Zhiyuan Tang³, Ning Bao⁵, Dong Ding⁶, Wenxuan Wu^{7*}, Fengru Fan^{8*}, Wenzhuo Wu^{1,2,9,10*}

¹School of Industrial Engineering, Purdue University, West Lafayette, Indiana 47907, USA

²Flex Laboratory, Purdue University, West Lafayette, Indiana 47907, USA

³Department of Applied Chemistry, School of Chemical Engineering and Technology, Tianjin University, Tianjin, 300072, China

⁴School of Electrical and Computer Engineering, Purdue University, West Lafayette, Indiana 47907, USA

⁵School of Public Health, Nantong University, Nantong, Jiangsu, 226019, China

⁶Energy & Environment Science and Technology, Idaho National Laboratory, Idaho Falls, Idaho 83415, USA

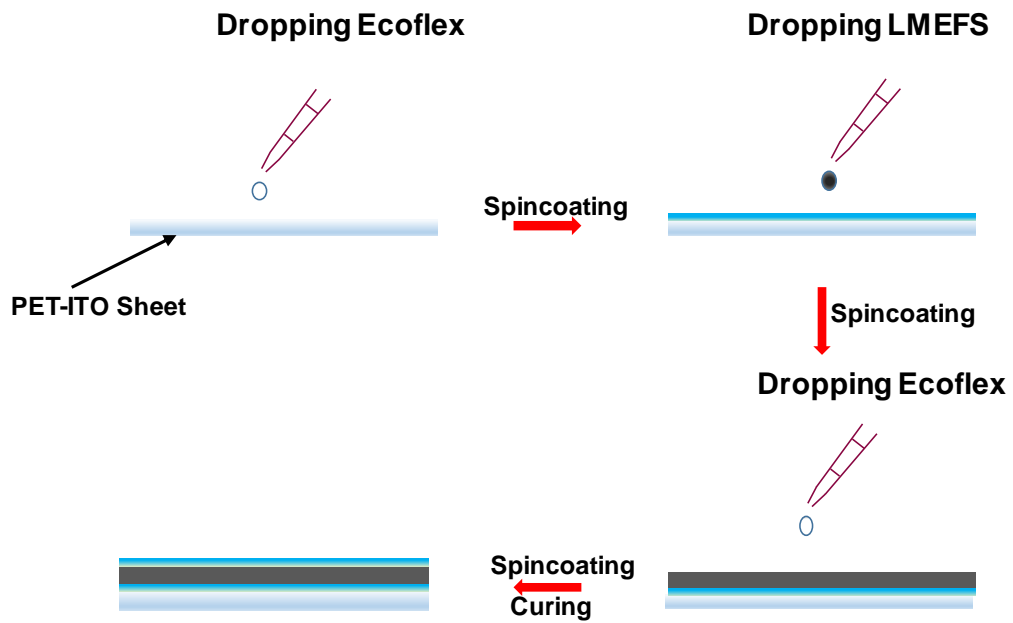
⁷Shenzhen Broadthink Advanced Materials Technologies Co., Ltd., Shenzhen, Guangdong, 518117, China

⁸Department of Chemistry & Biochemistry, University of California, Santa Barbara, CA 93106, USA

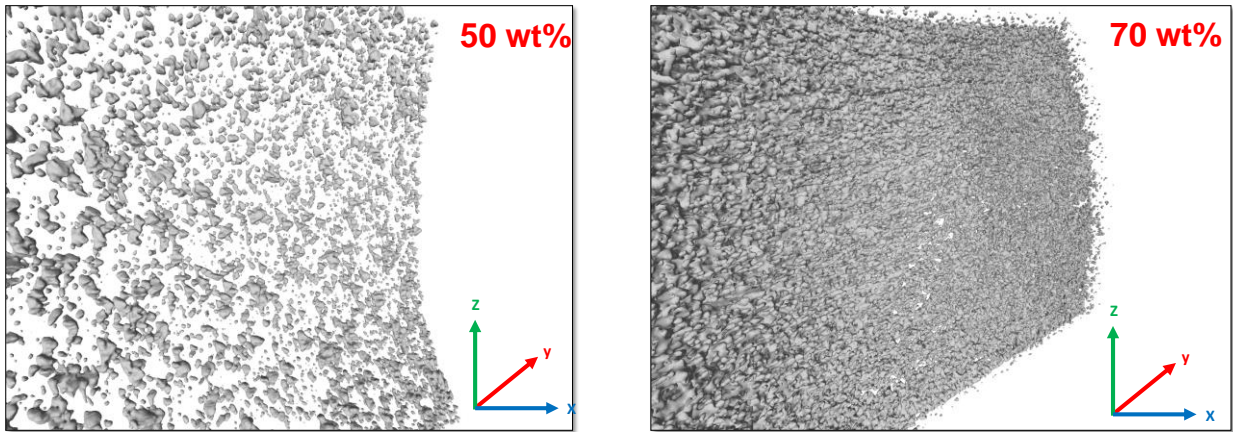
⁹Birck Nanotechnology Center, Purdue University, West Lafayette, Indiana 47907, USA

¹⁰Regenstrief Center for Healthcare Engineering, Purdue University, West Lafayette, Indiana 47907, USA

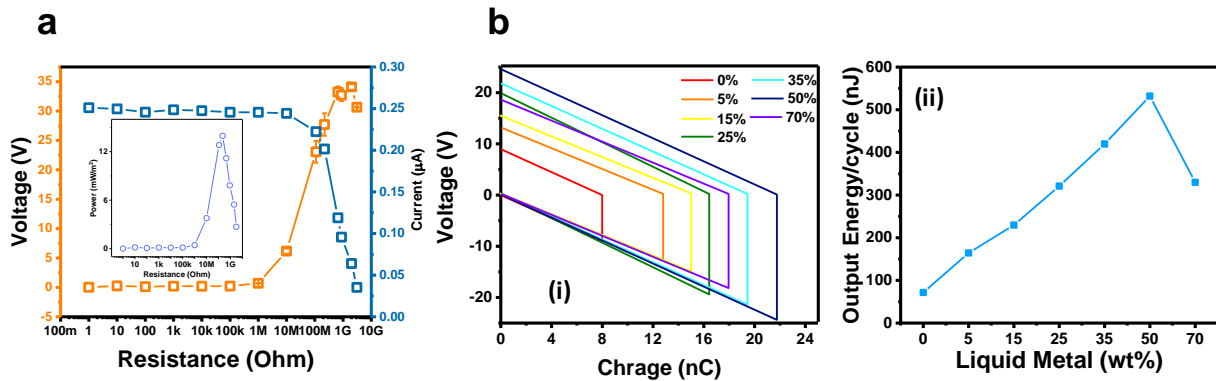
*e-mail: Correspondence and requests for materials should be addressed to W. Z. W (wenzhuowu@purdue.edu), F. R. F (fengrufan@ucsb.edu), or W. X. W (wxwu@mail.ustc.edu.cn)



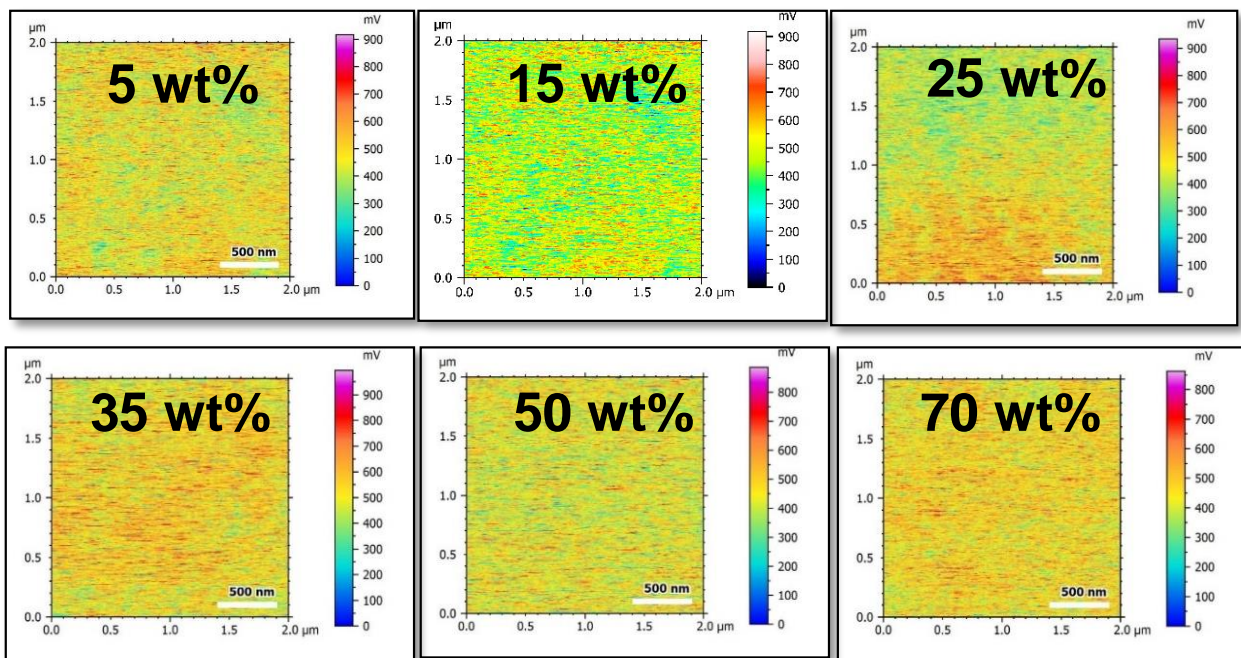
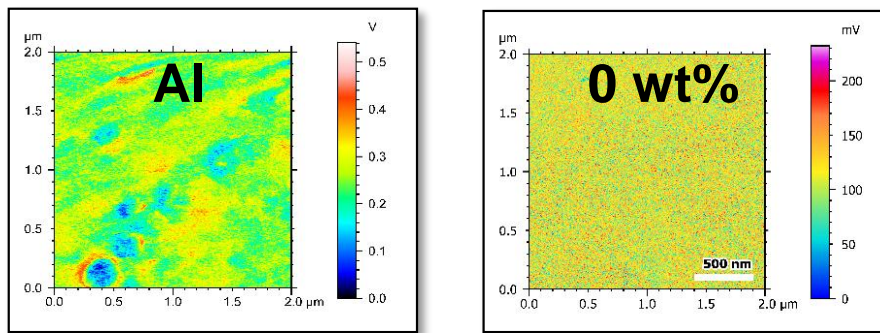
Supporting Figure 1 | Illustration of the fabrication of LMI-TENG with ITO electrode.



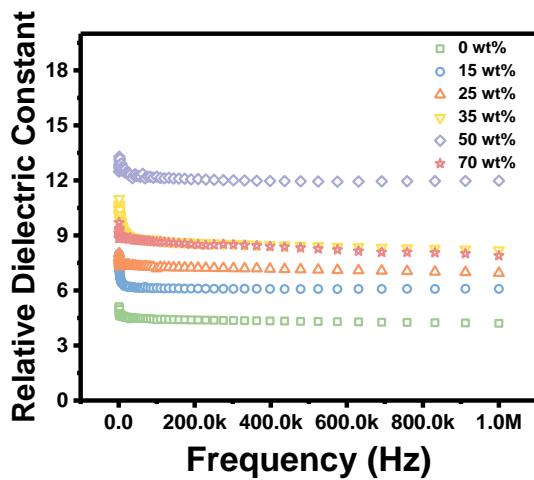
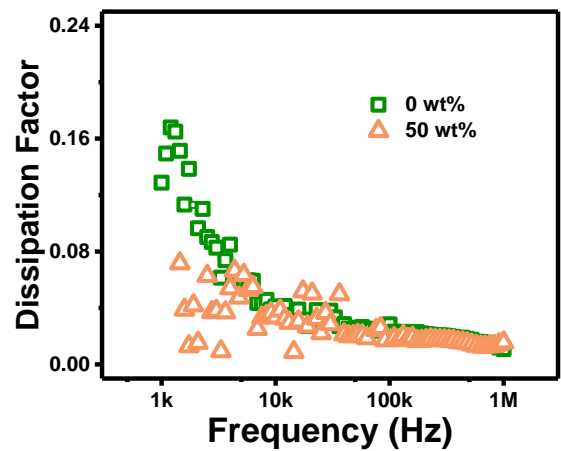
Supplementary Figure 2 | 3D Micro-CT results showing the shape and distribution of LMPs in two types of LMEFS.



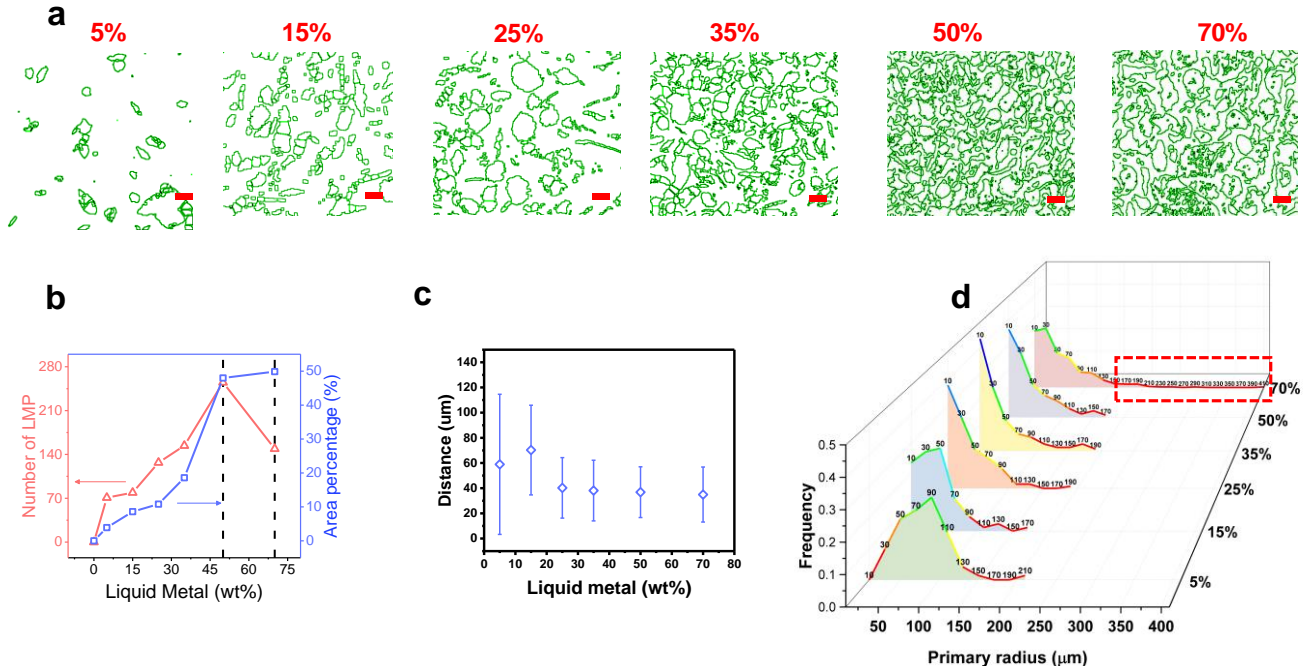
Supporting Figure 3 | LMI-TENG's output power measurement. (a) Voltage and Current output under different external loads. (b) The result of CMEO as a function of different wt% of LMPs in LMI-TENG.



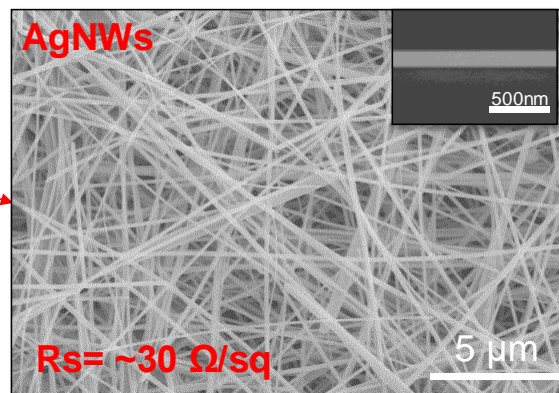
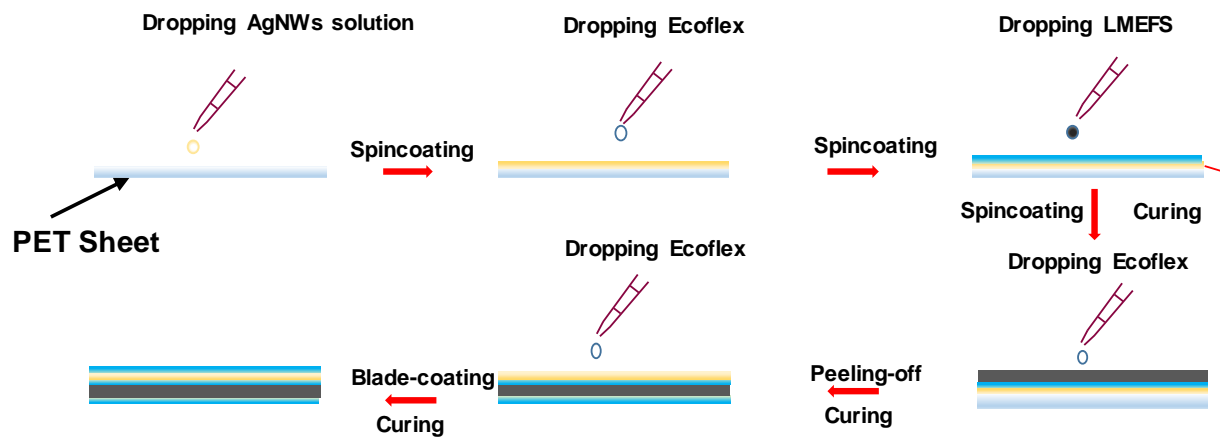
Supporting Figure 4 | Surface Potential of CL in Different Types of LMI-TENG. (a) The illustration of KPFM results of Al and different types of SDS. **(b)** The plot of surface potential of Al and CL as a function of different wt.% of LMPs.

a**b**

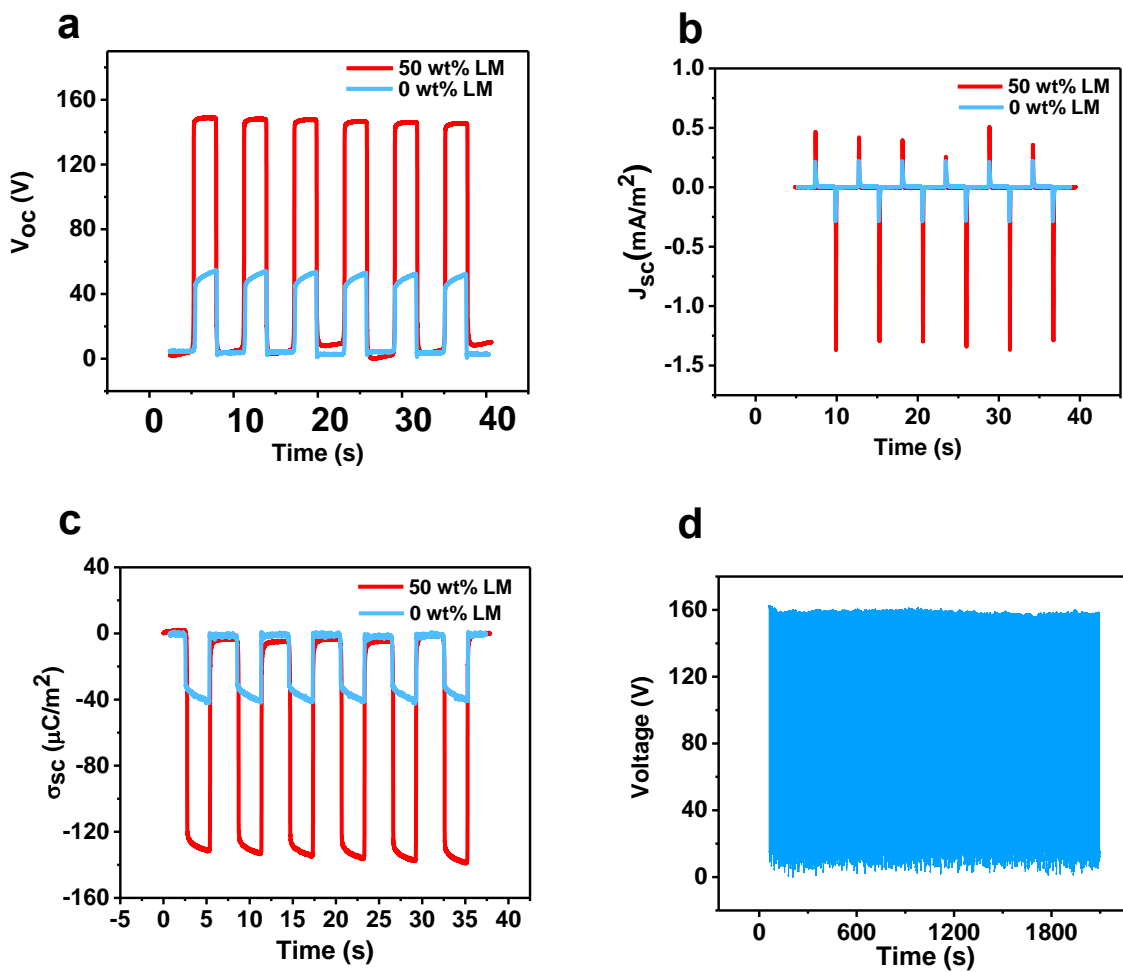
Supporting Figure 5 | LMI-TENG's dielectric measurement. (a) Dielectric constant of SDS with different wt.% of LMPs insides as a function of frequency showing that the dielectric constant is frequency independent. (b) Dissipation factors of SDS with 50% LM. and 0% Insides as a function of frequency showing that it was frequency independent.



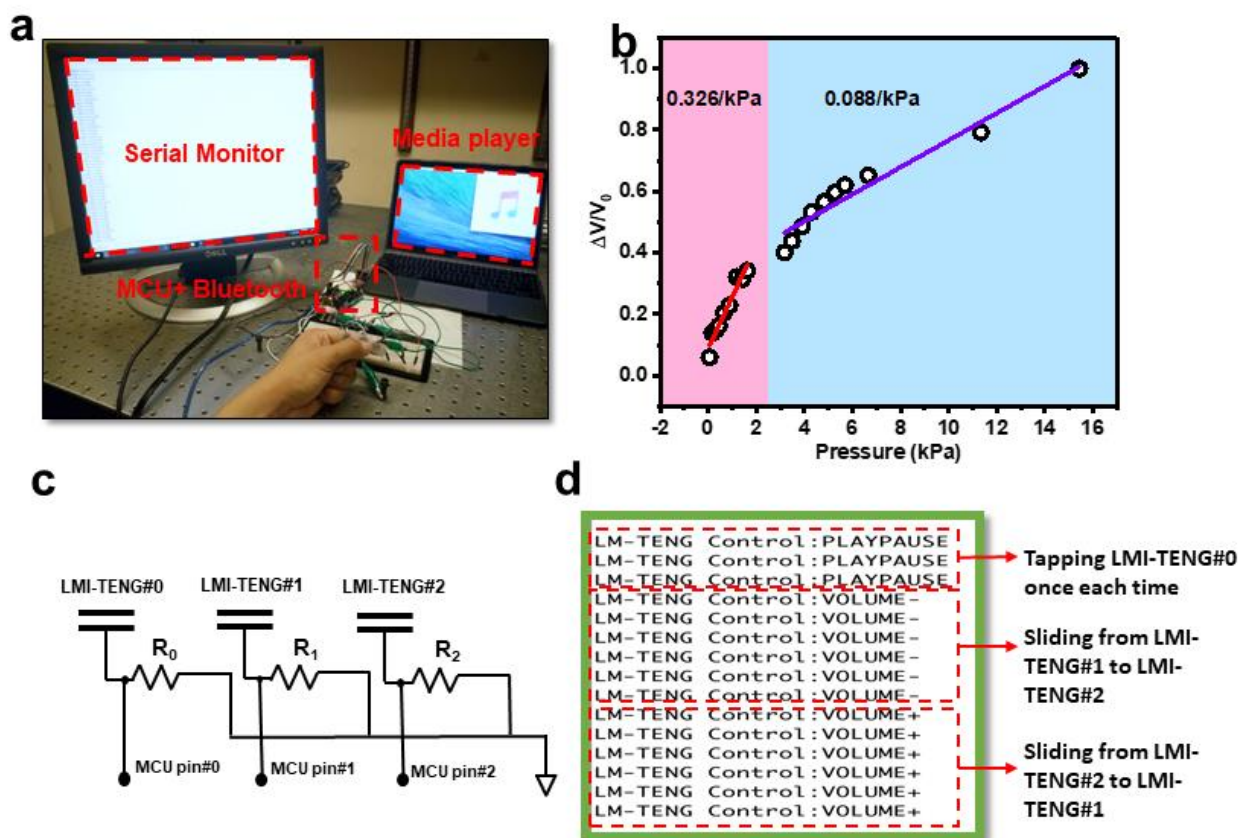
Supporting Figure 6 | Statistical result of the spatial distribution of LMPs inside LMEFS (a)-(b) Segmented image of the selected area of LMEFS, scale bar =100 μm and its corresponding distance distribution between two nearest LMPs. (c) The primary radius distribution of LMPs in different types of LMEFS. (d) The statistical result of the primary radius distribution for different LMEFS.



Supporting Figure 7 | Illustration of the fabrication of LMI-TENG with Ag NWs electrode.



Supporting Figure 8 | Working performance and mechanical stability of LMI-TENG with Ag NWs electrode. (a) Open-circuit Voltage. (b) Short-circuit Current density. (c) Short-circuit transferred charge density. (d) Mechanical Stability test.



Supporting Figure 9 | MCS demonstration (a) Illustration of LMI-TENG based MCS. **(b)** Pressure sensitivity of LMI-TENG with Ag NWs as electrode. **(c)** The diagram of the equivalent circuit of LMI-TENG based MCS. **(d)** Serial communication screenshot in LMI-TENG based MCS.